Journal of Molecular Catalysis A: Chemical 327 (2010) 73–79

Contents lists available at ScienceDirect

Journal of Molecular Catalysis A: Chemical

journal homepage: www.elsevier.com/locate/molcata

Investigation of the catalytic efficiency of a new mesoporous catalyst SnO_2/WO_3 towards oleic acid esterification

Arpita Sarkar[a], Sudip K. Ghosh[b], Panchanan Pramanik[a,*]

[a] Department of Chemistry, Indian Institute of Technology Kharagpur, Kharagpur, West Bengal 721302, India
[b] Department of Biotechnology, Indian Institute of Technology Kharagpur, Kharagpur, West Bengal 721302, India

ARTICLE INFO

Article history:
Received 2 February 2010
Received in revised form 4 May 2010
Accepted 23 May 2010
Available online 31 May 2010

Keywords:
Mesoporous
SnO_2/WO_3
Solid acid catalyst
Esterification
Oleic acid

ABSTRACT

The synthesis of a new, effective and reusable heterogeneous catalyst, mesoporous SnO_2/WO_3 (SW) to promote the esterification involving oleic acid and ethanol for the production of ethyl oleate is presented here. The developed mesoporous SnO_2/WO_3 with surface area of 130 m^2/g and pore size of 3.9 nm exhibits up to 90% conversion of oleic acid (for 2 h reaction, at 80 °C) with high yield (~92%) to the ethyl oleate, a product of the esterification reaction of oleic acid. The catalyst exhibits a comparable activity of H_2SO_4, which is a known catalyst for esterification of organic acids. Kinetic investigation reveals that the experimental data follows a first order dependency on the concentration of the oleic acid and the catalyst. The conversion of oleic acid also has noticeable dependency on the reaction temperatures and different alcohols. Regeneration through heating of the used mesoporous SnO_2/WO_3 catalyst at 400 °C for 3 h allows it for reuse without losing of its catalytic activity.

© 2010 Elsevier B.V. All rights reserved.

1. Introduction

In recent years, biodiesel consisting of methyl or ethyl esters of fatty acids are gaining increasing demands as a substitute for conventional petroleum derived diesel because of the increasing price of the later. The methyl or ethyl esters of fatty acids can be produced by the esterification of fatty acids. For the production of fatty acid esters, biocatalysts [1–4] should be the useful examples in terms of exceptional selectivity but their low reaction rates, short cell life spans, inhibitor tolerance, difficulties in product separation and expensive sterile equipments increase the production cost and thus limit them for commercial application [5]. The homogeneous and heterogeneous catalysts are also employed for esterification reactions of fatty acid for the production of fatty acid ester. Among the homogeneous catalysts sulfuric acid, methane sulfonic acid, *p*-toluene sulfonic acid are the most common acid catalysts. Basic catalysts are on the other hand not favorable for the production of fatty acid esters owing to the disadvantages such as high sensitivity of the catalysts to water and free fatty acids [6,7] and formation of the soap [8]. Formation of soap lowers the yield of esters and makes the separation of esters difficult. Besides, the base catalyzed reaction requires the use of expensive refined oils that should have low free fatty acids content (inferior to 0.5 wt%) [9,10]. Apart from these catalysts, many organo tin compounds are also used as homogeneous catalyst in fatty acid esterifications [11]. In spite of several advantages, homogeneous catalysts have some limitations which include problem in recovering the catalysts, disposal of toxic wastes formed during reactions, separation of the products, and loss of catalysts. So, an effective, environmentally benign, low cost production of biodiesel extensively demands solid heterogeneous catalysts. The recent works on the esterifications of free fatty acids to produce biodiesels involve the use of different heterogeneous inorganic catalysts such as, zeolite [12–14], heteropolyacids [15,16], ion exchange resin [14,17,18], carbon based material [14,15], sulfated ZrO_2 [14,19], sulfated TiO_2 [19], sulfated SnO_2 [19], and $Nb_2O_5.5H_2O$ [19], WO_3/ZrO_2 [20,21], tungstophosphoric acid [22], tungstosilicic acid [22] and molybdophosphoric acid immobilized on SiO_2 [22], propylsulfonic acid functionalized mesoporous SiO_2 [23,24], SnO [25], etc. However, to our knowledge the mesoporous SnO_2/WO_3 has not yet been explored as a catalyst. Although in the last decade $SnWO_4$ and SnO_2/WO_3 were insinuated as gas sensors the synthesis of mesoporous SnO_2/WO_3 and its catalytic behavior have not been reported so far.

Aiming this inadequacy, in the present manuscript, we report the synthesis of mesoporous SnO_2/WO_3 (SW) using stannous chloride and sodium tungstate as precursor compounds in presence of an anionic surfactant, sodiumdodecyl sulfate. The catalytic behavior of mesoporous SW has been examined in the esterification of oleic acid with ethanol to produce ethyl oleate for the first time. In this study, the optimization of the reaction has been done and reusability of the catalyst has also been checked. We have found

* Corresponding author. Tel.: +91 3222 283322; fax: +91 3222 255303.
E-mail address: panchanan_123@yahoo.com (P. Pramanik).

1381-1169/$ – see front matter © 2010 Elsevier B.V. All rights reserved.
doi:10.1016/j.molcata.2010.05.015

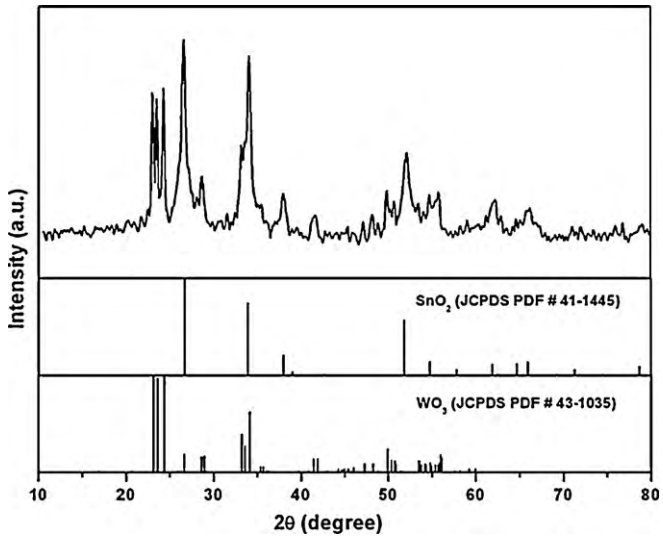

Fig. 1. High angle XRD patterns of mesoporous SW calcined at 500 °C for 4 h.

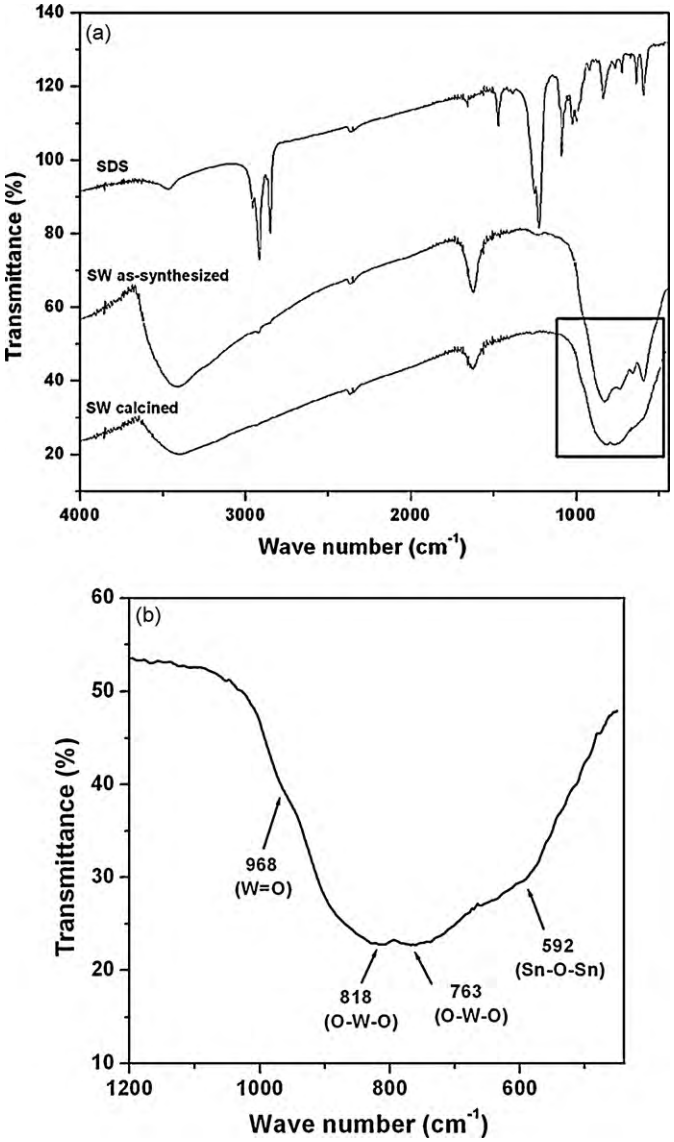

Fig. 2. (a) Combined FTIR spectra of the surfactant, as-synthesized SW and calcined mesoporous SW and (b) selected portion of the FTIR spectrum of calcined SW.

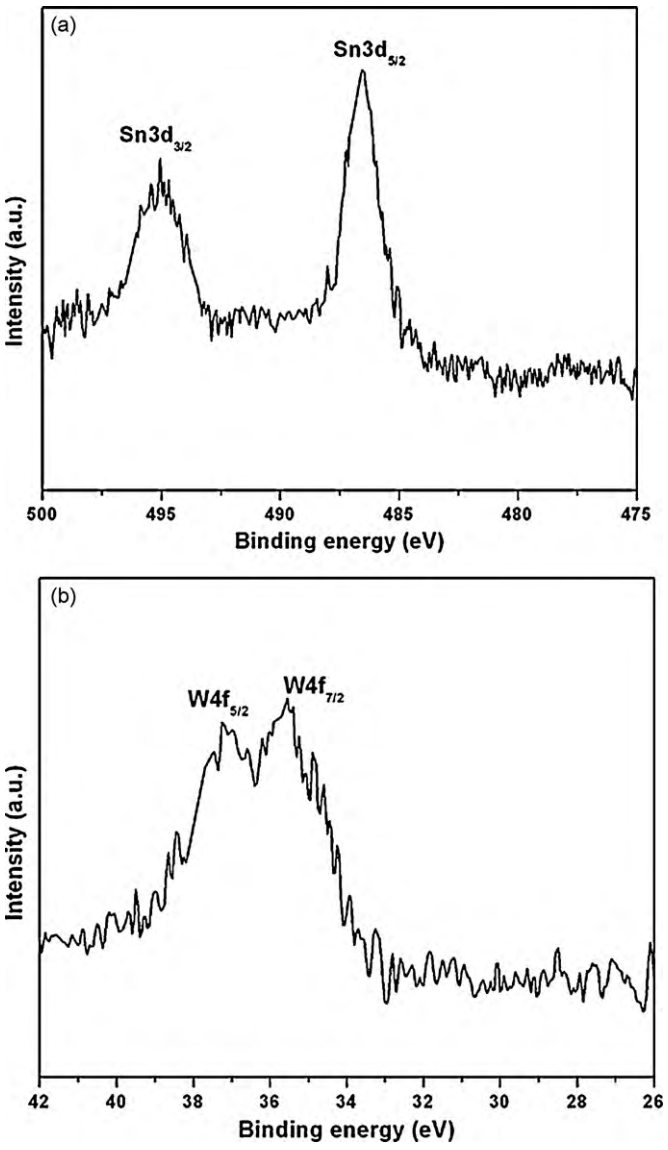

Fig. 3. X-ray photoelectron spectra of (a) Sn 3d core level and (b) W 4f core level of mesoporous SW calcined at 500 °C for 4 h.

that the mesoporous SW shows high conversion of oleic acid following pseudo first order kinetics.

2. Experimental

2.1. Reagents

Stannous chloride ($SnCl_2$), hydrochloric acid (HCl), hydrogen peroxide (H_2O_2) and sodium tungstate (Na_2WO_4) were procured from E. Merck (India). Sodiumdodecyl sulphate (SDS) was obtained from Sisco research laboratory.

2.2. Synthesis of mesoporous SnO_2/WO_3

In a typical synthesis 4.5 g of $SnCl_2$ was dissolved in 20 ml distilled water after addition of 10 ml concentrated HCl to it. To this solution, 6.2 ml H_2O_2 was added and stirred. Under stirring condition, this solution was mixed well with the aqueous solution of SDS which was prepared before by dissolving 1.72 g of SDS in 12 ml distilled water. An aqueous solution of Na_2WO_4 prepared by dissolving 11.8 g of Na_2WO_4 in 30 ml distilled water was then added

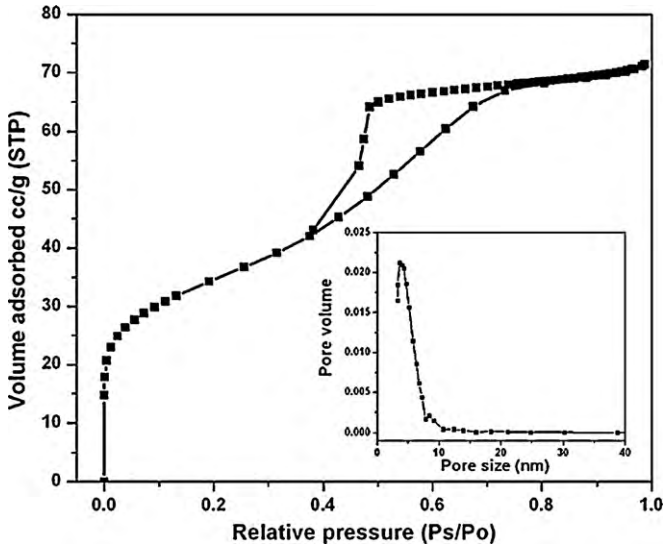

Fig. 4. N_2 adsorption–desorption isotherms of mesoporous SW calcined at 500 °C for 4 h and (inset) the corresponding BJH pore size distribution.

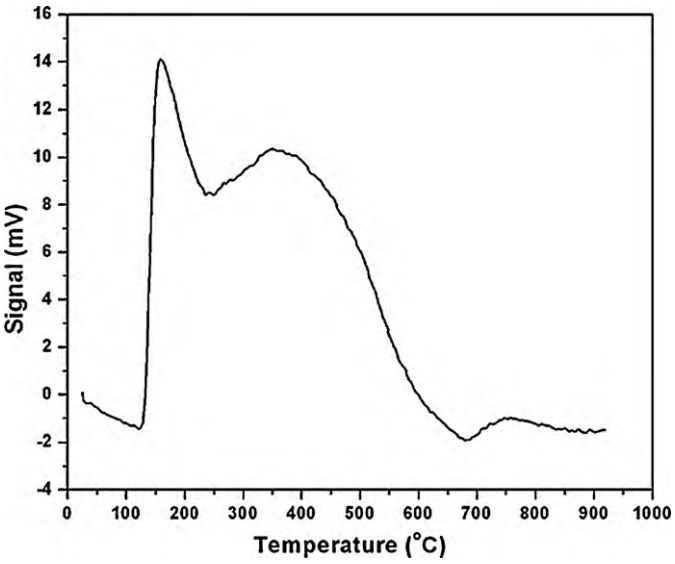

Fig. 6. NH_3 temperature-programmed desorption curve of mesoporous SW calcined at 500 °C for 4 h.

slowly by a small portion at a time to the well-mixed solution mixture under constant stirring condition. After complete addition of Na_2WO_4, the solution mixture was stirred for an additional 30 min. After that, the resultant solution was set aside for 24 h for complete precipitation. Pale yellow gel type precipitate was formed which was aged in Teflon lined autoclave at 120 °C for 24 h. The autoclave was cooled and the precipitate was filtered, washed thoroughly with distilled water to make free from Cl^- and then dried at 100 °C. The as-synthesized sample was finally calcined at 500 °C for 4 h to remove the surfactant.

2.3. Characterization techniques

Fourier transform infrared (FTIR) spectra were obtained on a Thermo Nicolet NEXUS 870 FTIR spectrometer. The calcined SW powder at 500 °C for 4 h was analyzed by X-ray powder diffraction using an X'Pert-pro Diffractometer operated at 40 kV and 25 mA and Cu Kα radiation and Ni filter. Analysis was performed at room temperature under vacuum to minimize air scatter. The data were collected over the 2θ angle range of $10^\circ \leq 2\theta \leq 80^\circ$. The BET (Brunauer–Emmett–Teller) surface area of the calcined SW powder (after out-gassing the powders at 200 °C for 4 h) was determined through N_2 adsorption–desorption study performed at liquid N_2 temperature using Beckman Coulter SA3100 surface area analyzer. The pore size distribution curve was obtained from the analysis of the adsorption branch of the isotherm by the BJH (Barrett–Joyner–Halenda) method. The surface morphology was studied using a JEOL-JSM6500 scanning electron microscope (SEM). The high resolution transmission electron microscopy (HRTEM) study was carried out using JEOL 2010 (ultrahigh-resolution model, equipped with a Gatan multi-scan CCD camera). For the HRTEM experiment, the sample was prepared by suspending the calcined powder in ethyl alcohol by sonication and taking a drop of the suspension on 200-mesh carbon coated copper grid. X-ray photoelectron spectra (XPS) analyses were carried out using a VG Scientific (ESCALAB 250) X-ray photoelectron spectrometer with an Al Kα X-ray source (1486.6 eV) at a base pressure of 2×10^{-9} Torr and all the spectra were curve fitted using bands with a Gaussian–Lorentzian line shape and a Shirley baseline. To determine the surface acidity by temperature-programmed desorption (TPD) of ammonia a Quantachrome CHEMBET-3000 instrument interfaced to a computer was used. The computer was employed to perform the programmed heating and cooling cycles, data recording, data valve switching, data storage and analysis. Before the TPD study, the sample was treated at 200 °C for 1 h in helium flow (50 cm^3/min) and then the sample was cooled to ambient temperature and saturated with high purity anhydrous ammonia (80 cm^3/min) for 1 h. The sample was then heated to 105 °C

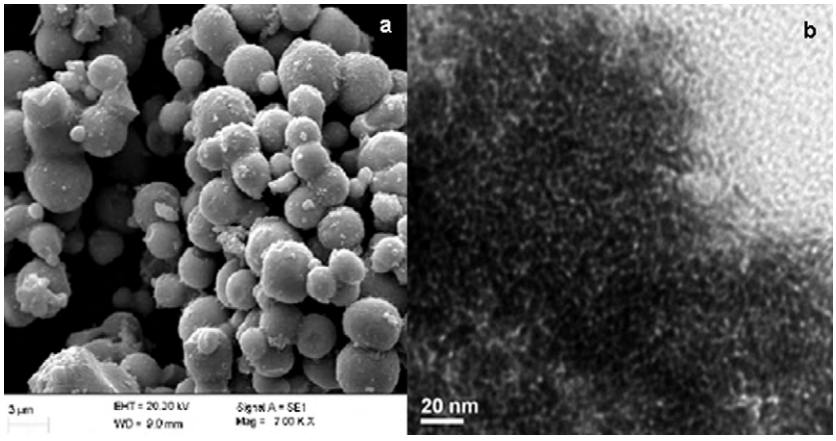

Fig. 5. (a) SEM micrograph and (b) bright field TEM micrograph of mesoporous SW calcined at 500 °C for 4 h.

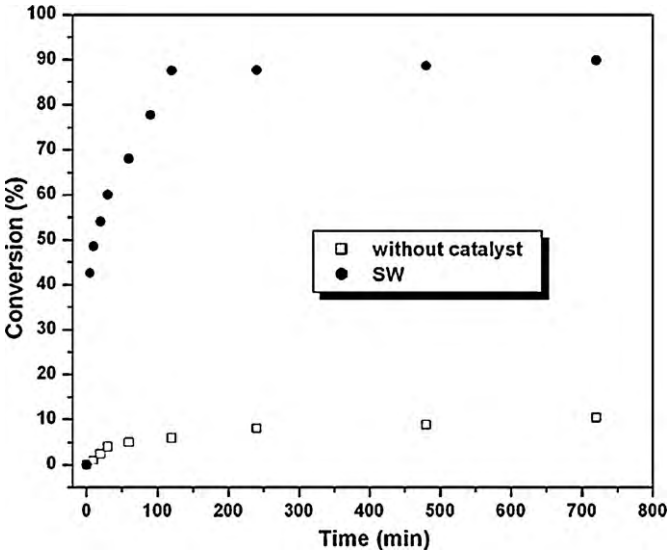

Fig. 7. Esterification of oleic acid in presence of 0.1 g mesoporous calcined SW and in absence of catalyst. *Reaction conditions*: reaction temperature = 80 °C, molar ratio of oleic acid:ethanol = 1:120, reaction time = 12 h.

and flushed with helium (50 cm^3/min) at the same temperature to remove the physisorbed ammonia. TPD analysis was carried out from ambient temperature to 900 °C.

2.4. General procedure of catalytic test

The esterification reaction of oleic acid was carried out in a three-necked round bottom flask, equipped with a reflux condenser, a thermometer and a sampling system. The whole system was kept in an oil bath which was placed upon a magnetic stirrer. In a typical catalytic reaction, 120 mmol ethanol and 1 mmol oleic acid were reacted in presence of 0.1 g (1.7 wt% calculated following the expression of (amount of catalyst in g × 100/amount of (oleic acid + ethanol) in g)) of mesoporous SW in a round bottom flask at different temperatures under continuous stirring. All the catalytic tests were performed in triplicate to examine the reproducibility of the result. In this study, the esterification of oleic acid with ethanol was also carried out in absence of mesoporous SW,

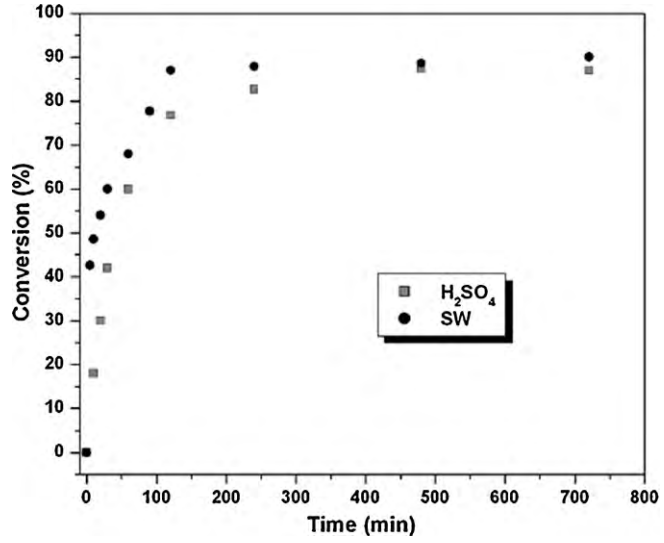

Fig. 8. Esterification of oleic acid in presence of H_2SO_4 and 0.1 g mesoporous calcined SW. *Reaction conditions:* reaction temperature = 80 °C, molar ratio of oleic acid:ethanol = 1:120, reaction time = 12 h.

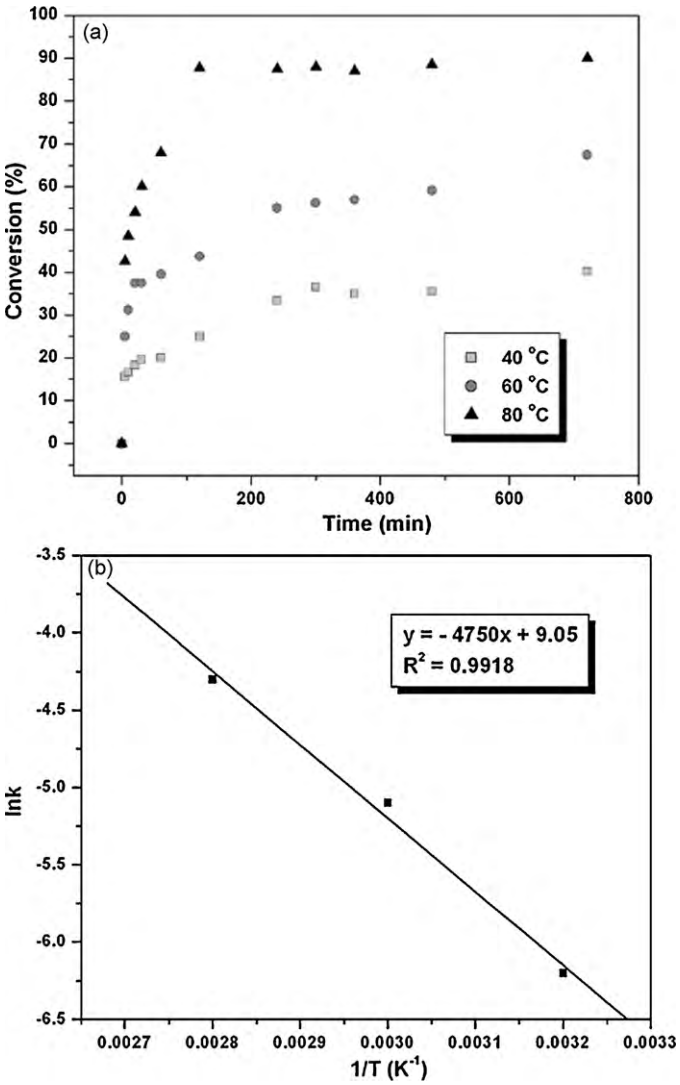

Fig. 9. (a) Esterification of oleic acid executed at different temperatures (40, 60 and 80 °C) in presence of 0.1 g mesoporous calcined SW. *Reaction conditions*: molar ratio of oleic acid:ethanol = 1:120, reaction time = 12 h. (b) Plot of ln *k* vs. 1/*T* for the esterification of oleic acid and ethanol using mesoporous SW (from initial reaction rate data).

in presence of different amounts of mesoporous SW, and also in presence of 0.1 mol H_2SO_4, which is a known catalyst for esterification of organic acids. The influence of the reaction temperature and the effect of different alcohols have also been investigated in the esterification of oleic acid, catalyzed by the mesoporous SW. The conversion of the oleic acid to the ethyl oleate was determined by titration of the aliquots, taken out from the reaction mixture at different time intervals with a standard (0.01 M) alcoholic solution of KOH and the reaction was also monitored by gas chromatography (GC) analysis of the aliquots taken at regular interval. Prior to titration as well as GC analysis, the catalyst was separated from the aliquot of reaction mixture through centrifugation to inhibit further reaction. The yield of ethyl oleate formed in the catalytic reaction was calculated from the GC peak area of the ethyl ester in comparison to the corresponding analytical curve. The GC analysis was done using Shimadzu GC-17A instrument (with FID detector), equipped with a 30 m × 0.25 mm DB-1 column at a temperature range of 80–180 °C with a heating rate of 10 °C/min.

3. Results and discussions

3.1. Characterization

XRD and FTIR studies have been carried out to elucidate the structural properties of the synthesized mesoporous SW. Fig. 1 displays the XRD of the mesoporous SW calcined at 500 °C for 4 h. The XRD profile shows that the mesoporous material possesses mixture of tetragonal SnO_2 (JCPDS PDF #41-1445 cassiterite, syn) and monoclinic WO_3 (JCPDS PDF #43-1035). Thus the XRD study reveals the coexistence of SnO_2 and WO_3 resulting a composite oxide. FTIR spectra of the surfactant (SDS), as-synthesized SW and calcined SW are shown in Fig. 2a. As we observe no band corresponding to surfactant present in the FTIR of calcined SW, we can conclude from FTIR study that after calcination at 500 °C for 4 h SW lacks any surfactant. Absence of any surfactant is also supported by elemental analysis. In all FTIR spectra, the bands near 3432 and 1631 cm^{-1} (Fig. 2a) appear due to the presence of O–H and H–O–H species, respectively. Selected portion of the FTIR spectrum of calcined SW in Fig. 2a has been enlarged in Fig. 2b to show one absorption band centered at approximately 818 cm^{-1} along with an additional band at 763 cm^{-1}, which can be identified as the stretching frequency of O–W–O groups [26]. A less intense band appeared at 968 cm^{-1} can be attributed to the W=O group [26] whereas the band at 592 cm^{-1} can be assigned to the Sn–O–Sn of the tin oxide framework [27]. XPS analyses (Fig. 3) of the mesoporous SW calcined at 500 °C for 4 h gives information on the chemical composition as well as the chemical bonding states of Sn and W in the powder material. The Sn 3d core-level spectra (Fig. 3a) exhibits that two peaks correspond to Sn $3d_{5/2}$ and Sn $3d_{3/2}$ appear at 486.5 and 494.9 eV, respectively. These values of the peaks for the synthesized mesoporous SW are identical to the Sn(IV) oxide [28]. In addition, the photoelectron peaks (Fig. 3b) of W $4f_{7/2}$ and W $4f_{5/2}$, appeared at 35.3 and 37.4 eV respectively are identical to that of W(VI) oxide [28]. The surface compositions for our synthesized mesoporous SW obtained from XPS analysis shows the presence of 7.89% Sn and 14.17% W. The textural properties such as BET surface area and the pore diameter of the SW calcined at 500 °C for 4 h have been evaluated using the N_2 adsorption-desorption measurements at liquid N_2 temperature in a relative pressure range from 0.05 to 1.0. Fig. 4 exhibits the N_2 adsorption–desorption isotherm and the corresponding pore size distribution curve (Fig. 4, inset) of the synthesized SW calcined at 500 °C for 4 h. The shape of N_2 adsorption–desorption isotherm corresponds to type IV [29] indicating typical mesoporous nature of the sample. The BET surface area and the pore volume of the calcined SW are found to be 130 m^2/g and 0.198 cm^3/g, respectively. The porous texture of the calcined SW was analyzed and the pore size distribution was measured through BJH method from the adsorption branch of the isotherm. The pore size distribution, centered at 3.9 nm, is uniform but a small fraction of pores are present in the range of >3.92 and10 nm, probably due to thermal collapse of the pore structure of the calcined samples. The morphology of the mesoporous SW calcined at 500 °C for 4 h, investigated by scanning electron microscopy is shown in Fig. 5a. SEM image shows the powder material being composed of largely spherical particles. The HRTEM micrograph of mesoporous SW calcined at 500 °C for 4 h (Fig. 5b) depicts the uniform porous network in the mesoporous range with open-pore structure of 3–4 nm diameter pores in an unordered array. The pores appear to be worm-like as evident from the HRTEM micrograph. The ammonia temperature-programmed desorption method which is a conventional method for characterizing the surface acidity in mesoporous materials, has been used for determining the acid strength distribution of the mesoporous SW. The acid strength distribution is indicated by the temperature range at which most of the ammonia desorbed [30,31]. Fig. 6 indicates the temperature-programmed desorption curve of mesoporous SW. This curve shows that one well-resolved desorption peak of NH_3 appears at 158 °C which is attributed to NH_3 adsorbed on weak acid sites. A broad desorption signal (at the range of 250–650 °C) likely centered at around 350 °C appears corresponding to the NH_3 adsorbed on medium-strong acid sites.

3.2. Catalytic activity

3.2.1. Esterification reaction of oleic acid

In the present study catalytic performance of the synthesized mesoporous SW and the dependency of its catalytic efficiency on different reaction parameters for the esterification of oleic acid with ethanol has been investigated.

The esterification of oleic acid with ethanol generally proceeds via formation of ethyl oleate and water as given below.

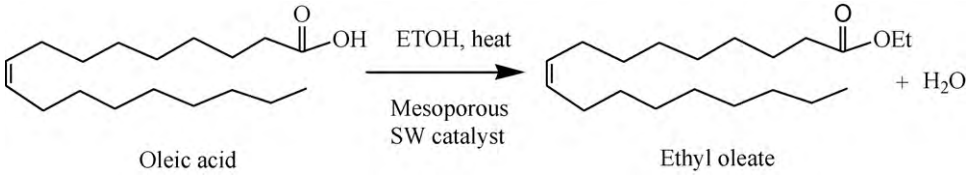

In a typical esterification reaction, molar ratio of ethanol to oleic acid has been maintained at 120:1. The esterification reaction is an equilibrium reaction. To achieve a high conversion of oleic acid a high ethanol-to-oleic acid molar ratio has been employed [32]. The esterification reaction executed at 80 °C for 2 h in presence of 0.1 g mesoporous SW gives rise to ~90% conversion (Fig. 7) of oleic acid into ethyl oleate and the corresponding yield of ethyl oleate has been found to be ~92%. While the same reaction performed at 80 °C for 2 h in absence of any catalyst produces only ~10% conversion (even after 12 h reaction, Fig. 7). The same experiment has been repeated using a well-known catalyst H_2SO_4 to compare the catalytic efficiency of our catalyst. In this study, we have found as shown in Fig. 8 that the mesoporous SW achieves the similar efficiency of H_2SO_4 in conversion (~90%) of oleic acid into ethyl oleate. As is observed from the experiment that in presence of the catalyst, the conversion of oleic acid in esterification reaction significantly speed up within the initial 2 h and after 2 h, the conversion reaches saturation where it remains almost invariable. The catalytic tests have been carried out in triplicate to examine the reproducibility of the results and presented the average results which accord the experimental results obtained by GC analysis.

3.2.2. Effect of different reaction conditions on the reaction

3.2.2.1. The effect of the reaction temperature. Three reaction temperatures such as 40 °C, 60 °C and 80 °C have been selected to investigate the influence of reaction temperatures on the mesoporous SW catalyzed esterification of oleic acid with ethanol. The conversion of oleic acid into ethyl oleate via esterification has noticeable dependency on the reaction temperatures as seen in the Fig. 9a. Fig. 9a shows that the oleic acid conversion increases from 40 to 67 to 90% as the temperature increases from 40 to 60 to 80 °C. The increased conversion might be not only due to the effect of increase of the reaction rate by increasing temperatures but also some improvement of the mass transfer limitation between reactant and catalyst [22].

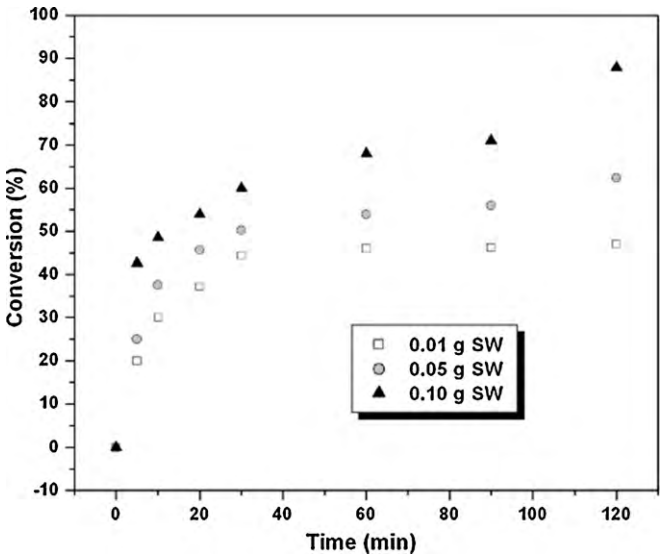

Fig. 10. Esterification of oleic acid in presence of different amount of mesoporous calcined SW (0.01, 0.05, 0.1 g). *Other reaction conditions*: reaction temperature = 80 °C, molar ratio of oleic acid:ethanol = 1:120, reaction time = 2 h.

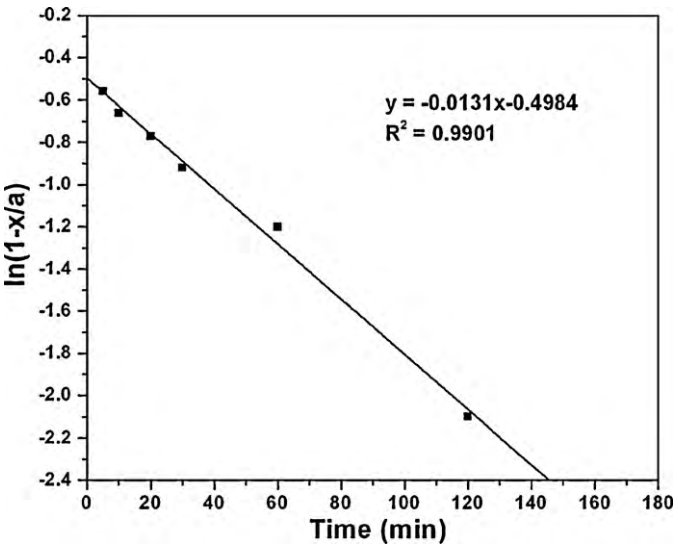

Fig. 11. Plot of $\ln(1 - x/a)$ vs. time. *Reaction conditions*: reaction temperature = 80 °C, molar ratio of oleic acid:ethanol = 1:120, amount of catalyst = 0.1 g, reaction time = 2 h.

The activation energy (E_a) has been calculated from the plot of $\ln k$ versus $1/T$ (Fig. 9b), constructed from the data obtained at each temperature of the reaction following the Arrhenius equation as given below:

$$k = A \exp\left(\frac{-E_a}{RT}\right)$$

or

$$\ln k = \ln A - \frac{E_a}{RT}$$

where k is the rate constant and the T denote the reaction temperature in Kelvin. The value of activation energy has been found to be 39.5 kJ/mol.

3.2.2.2. The effect of the amount of mesoporous SW. The effect of catalyst loading on the esterification reactions has also been studied using different amount of mesoporous SW (0.01, 0.05 and 0.1 g). The results displayed in Fig. 10 show that the maximum oleic acid conversion (~90%) has been achieved in presence of 0.1 g mesoporous SW whereas in presence of 0.01 and 0.05 g catalyst the conversions are up to 47 and 62%, respectively. The increase in the conversion of oleic acid with the increasing catalyst amount is expected because total surface area of the catalyst is increased and also more catalytic active sites are available [33]. The convergence behavior to the same final conversion using different amount of catalyst has not been observed within the time duration of the experiment, which is 2 h for the present study.

3.2.2.3. The effect of oleic acid concentration. In the present study of the esterification of oleic acid with ethanol, the ethanol is used in excess amount compared to the oleic acid. Therefore, the concentration of ethanol can be considered to be constant throughout the reaction duration and thus the reaction should follow the pseudo first order kinetic model [34]. Therefore, the rate constant can be expressed by the following equation:

$$k_R = -\frac{1}{tb} \ln \frac{a-x}{a} = -\frac{1}{tb} \ln\left(1 - \frac{x}{a}\right)$$

or

$$\ln\left(1 - \frac{x}{a}\right) = -k_R bt = -kt$$

where k = rate constant of the pseudo first order reaction, a = concentration of oleic acid, b = concentration of ethanol, x/a = conversion, t = time. So, the plot of $\ln(1 - x/a)$ versus t should produce a straight line and the pseudo first order rate constant (k) can be calculated from the slope of this plot. Fig. 11 presents the plot of $\ln(1 - x/a)$ versus time for the esterification reaction of oleic acid at 80 °C catalyzed by 0.1 g mesoporous SW and it indicates that the data are well fitted to this model exhibiting a straight line, confirming the esterification of oleic acid in this study, follows pseudo first order kinetics. The rate constant evaluated from the slope of the above plot for the esterification is found to be 0.0131 min^{-1}.

3.2.3. The esterification of oleic acid with different alcohols

Finally, the esterification of oleic acid has been carried out with propanol and butanol at 80 °C for 2 h in presence of 0.1 g mesoporous SW and the molar ratio of oleic acid:alcohol has been maintained at 1:120. The conversion of oleic acid with different alcohols is depicted in Fig. 12. It can be seen from Fig. 12 that the conversion of oleic acid decreases from ethanol to the higher alco-

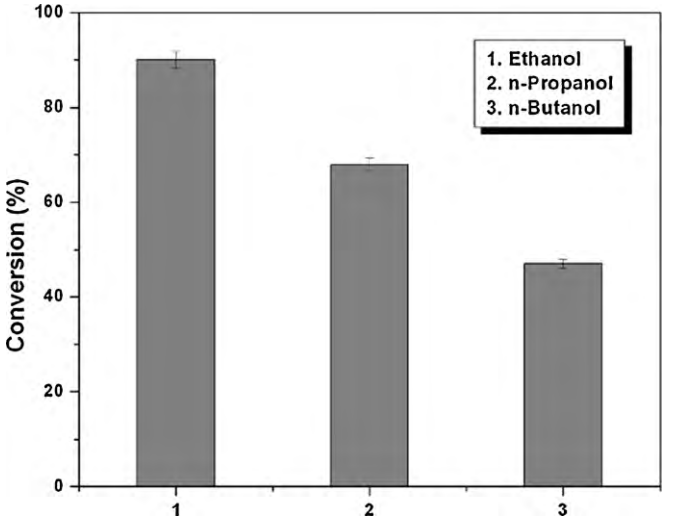

Fig. 12. Esterification of oleic acid executed with different alcohols. *Reaction conditions*: reaction temperature = 80 °C, molar ratio of oleic acid:alcohol = 1:120, amount of catalyst = 0.1 g, reaction time = 12 h.

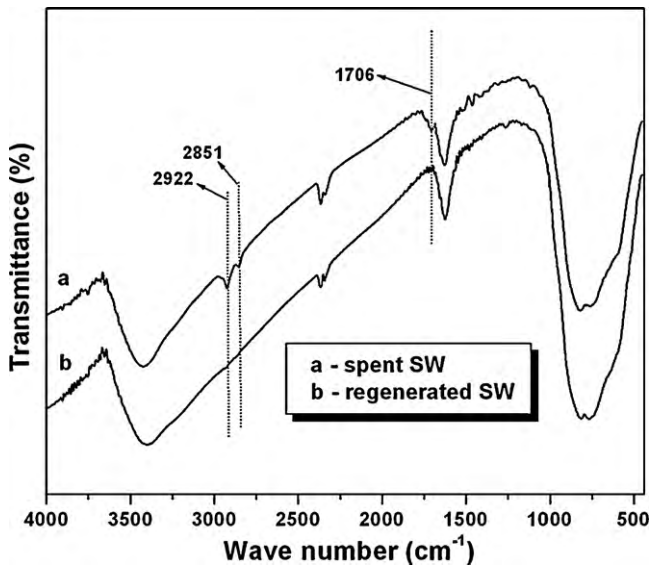

Fig. 13. FTIR spectra of the (a) spent mesoporous SW and (b) fresh mesoporous SW catalyst.

Table 1
EDX data of the fresh SW and regenerated mesoporous SW after the esterification reaction.

Type of catalyst	Fresh mesoporous SW	Regenerated mesoporous SW
Molar ratio of Sn/W	1.98	1.96

hols. Since, the molar mass of alcohol influences the diffusion rate and the reaction rate is linearly dependent on the diffusion rate, therefore, with the increase in molar mass from ethanol to butanol the reaction rate decreases for the decrease in diffusion rate and the conversion of oleic acid also decreases from ethanol to propanol to butanol within the reaction time limit. Beside, the chain length of the alcohol also influences in the steric hindrance for the nucleophilic attack to the polarized carbonyl centre of the oleic acid and thus reduces the extent of esterification [35].

3.2.4. Catalyst regeneration and reuse of the spent catalyst

After a catalytic reaction the spent catalyst has been analyzed by FTIR spectroscopy (Fig. 13a), which exhibits the appearance of an additional band at ~1706 cm^{-1} that should correspond to the C=O group and two prominent bands between 2800 and 3000 cm^{-1} for the C–H– stretching. These bands appear due to the adsorbed reagent or the product. For reusing, after a run, the spent mesoporous SW catalyst has been separated from the liquid product by centrifugation and after washing with distilled water regenerated by heating at 400 °C for 3 h which shows complete disappearance of the bands corresponding to the C=O and C–H stretches (Fig. 13b). The regenerated mesoporous SW has been used for five more runs to examine its reusability and found that the reused catalyst is very efficient to that of the fresh catalyst in formation of ethyl ester. EDX analysis of W content in fresh and regenerated catalyst (Table 1) shows that the activity of the spent catalyst could be regenerated completely as there is almost no loss of WO_3 after the reaction.

4. Conclusion

In the present study, a new heterogeneous solid acid catalyst mesoporous SnO_2/WO_3 composite with BET surface area of 130 m^2/g and average pore size of 3.9 nm has been synthesized and employed successfully in esterification of oleic acid with ethanol to produce ethyl oleate. The ethyl oleate is an important constituent of biodiesels. The synthesized mesoporous SnO_2/WO_3 exhibits ~90% conversion of oleic acid and the corresponding yield of ethyl oleate has been achieved to ~92%. The catalyst has been recovered after the catalytic test and regenerated by heating at 400 °C for 3 h and successfully reused in the same esterification reaction. The mesoporous SnO_2/WO_3 can be used for the production of different fatty acid esters through the acid catalyzed conversion of biorenewable lipid feedstocks, i.e., the free fatty acids.

Acknowledgement

AS greatly acknowledge CSIR, New Delhi, for providing the grants to support the completion of this work.

References

[1] N.W. Li, M.H. Zong, H. Wu, Process Biochem. 44 (2009) 685–688.
[2] R. Fernandez-Lafuente, J. Mol. Catal. B: Enzymatic 62 (2010) 197–212.
[3] S. Arai, K. Nakashima, T. Tanino, C. Oginoa, A. Kondo, H. Fukuda, Enzyme Microbial Technol. 46 (2010) 51–55.
[4] H. Fukudaa, A. Kondo, S. Tamalampudi, Biochem. Eng. J. 44 (2009) 2–12.
[5] I.K. Mbaraka, B.H. Shanks, J. Am. Oil Chem. Soc. 3 (2006) 79–91.
[6] L. Bournay, D. Casanave, B. Delfort, G. Hillion, J.A. Chodorge, Catal. Today 106 (2005) 190–192.
[7] M. Kouzu, S. Yamanaka, J. Hidaka, M. Tsunomori, Appl. Catal. A: Gen. 355 (2009) 94–99.
[8] E. Lotero, Y. Liu, D.E. Lopez, K. Suwannakarn, D.A. Bruce, J.G. Goodwin, Ind. Eng. Chem. Res. 44 (2005) 5353–5363.
[9] A. Baig, F.T.T. Ng, Energy Fuels, doi:10.1021/ef901258b.
[10] E. Lotero, Y. Liu, D.E. Lopez, K. Suwannakarn, D.A. Bruce, J.G. Goodwin Jr., Ind. Eng. Chem. Res. 44 (2005) 5353–5363.
[11] D.A.C. Ferreira, M.R. Meneghetti, S.M.P. Meneghetti, C.R. Wolf, Appl. Catal. A: Gen. 317 (2007) 58–61.
[12] T. Okuhara, Chem. Rev. 102 (2002) 3641–3666.
[13] S.R. Kirumakki, N. Nagaraju, S. Narayanan, Appl. Catal. A: Gen. 273 (2004) 1–9.
[14] A.A. Kiss, A.C. Dimian, G. Rothenberg, Adv. Synth. Catal. 348 (2006) 75–81.
[15] T. Okuhara, Catal. Today 73 (2002) 167–176.
[16] H. Matsuda, T. Okuhara, Catal. Lett. 56 (1998) 241–243.
[17] M.A. Harmer, W.E. Farneth, Q. Sun, J. Am. Chem. Soc. 118 (1996) 7708–7715.
[18] M.A. Harmer, Q. Sun, A.J. Vega, W.E. Farneth, A. Heidekum, W.F. Hoelderich, Green Chem. 2 (2000) 7–14.
[19] A.A. Kiss, A.C. Dimian, G. Rothenberg, Energy Fuels 22 (2008) 598–604.
[20] Y.-M. Park, D.-W. Lee, D.-K. Kim, J.-S. Lee, K.-Y. Lee, Catal. Today 131 (2008) 238–243.
[21] Y.-M. Park, J.Y. Lee, S.-H. Chung, I.S. Park, S.-Y. Lee, D.-K. Kim, J.-S. Lee, K.-Y. Lee, Bioresour. Technol. 101 (2010) S59–S61.
[22] C.S. Caetano, I.M. Fonseca, A.M. Ramos, J. Vital, J.E. Castanheiro, Catal. Commun. 9 (2008) 1996–1999.
[23] J.A. Melero, L.F. Bautista, G. Morales, J. Iglesias, D. Briones, Energy Fuels 23 (2009) 539–547.
[24] I.K. Mbaraka, K.J. McGuire, B.H. Shanks, Ind. Eng. Chem. Res. 45 (2006) 3022–3028.
[25] Y. Wang, Y. Liu, C. Liu, Energy Fuels 22 (2008) 2203–2206.
[26] M. Deepa, N. Sharma, P. Varshney, S.P. Varma, S.A. Agnihotry, J. Mater. Sci. 35 (2000) 5313–5318.
[27] S. de Monredon, A. Cellot, F. Ribot, C. Sanchez, L. Armelao, L. Gueneauc, L. Delattre, J. Mater. Chem. 12 (2002) 2396–2400.
[28] H.-J. Ahn, H.-S. Shim, Y.-E. Sung, T.-Y. Seong, W.B. Kima, Electrochem. Solid-State Lett. 10 (2007) E27–E30.
[29] S.J. Gregg, K.S.W. Sing, Adsorption Surface Area and Porosity, Academic Press, London, 1982.
[30] C. Resini, T. Montanari, L. Nappi, G. Bagnasco, M. Turco, G. Busca, F. Bregani, M. Notaro, G. Rocchini, J. Catal. 214 (2003) 179–190.
[31] E. Selli, L. Forni, Micropor. Mesopor. Mater. 31 (1999) 129–140.
[32] D.E. López, J.G. Goodwin Jr., D.A. Bruce, S. Furuta, Appl. Catal. A: Gen. 339 (2008) 76–83.
[33] C.S.M. Pereira, S.P. Pinho, V.M.T.M. Silva, A.E. Rodrigues, Ind. Eng. Chem. Res. 47 (2008) 1453–1463.
[34] C.F. Oliveira, L.M. Dezaneti, F.A.C. Garcia, J.L. de Macedo, J.A. Dias, S.C.L. Dias, K.S.P. Alvim, Appl. Catal. A: Gen. 372 (2010) 153–161.
[35] A.L. Cardoso, S.C.G. Neves, M.J. da Silva, Energy Fuels 23 (2009) 1718–1722.